



# Polyamide thin-film composite membranes based on carboxylated polysulfone microporous support membranes for forward osmosis

Young Hoon Cho<sup>a</sup>, Jungim Han<sup>b</sup>, Sungsoo Han<sup>b</sup>, Michael D. Guiver<sup>a,c</sup>, Ho Bum Park<sup>a,\*</sup>

<sup>a</sup> Hanyang University, WCU Department of Energy Engineering, Seoul 133-791, Republic of Korea

<sup>b</sup> Samsung Advanced Institute of Technologies, Suwon 440-600, Republic of Korea

<sup>c</sup> National Research Council Canada, Ottawa, ON, Canada K1A 0R6

## ARTICLE INFO

### Article history:

Received 29 April 2013

Received in revised form

4 June 2013

Accepted 4 June 2013

Available online 13 June 2013

### Keywords:

Forward osmosis

Microporous membrane

Desalination

Carboxylated polysulfone

## ABSTRACT

Due to its simple process and low energy consumption, forward osmosis (FO) has gained significant attention in the fields of portable hydration bags, desalination, landfill leachate treatment, and brine concentration. However, current state-of-the-art reverse osmosis (RO) membranes show relatively low water fluxes in FO processes due to high internal concentration polarization (ICP) and high mass transfer resistance in commercially available microporous support membranes. In this study, carboxylated polysulfones (CPSFs) were synthesized via direct polysulfone (PSF) functionalization and considered as hydrophilic, mechanically stable microporous support membranes. The incorporation of hydrophilic groups into hydrophobic polymer backbones often reduces mechanical strength due to excessive water swelling. However, the mechanical properties of CPSFs (degree of substitution, DS=0.49–0.85) were similar to those of pristine PSF, and they retained their hydrophilic nature. Microporous CPSF membranes were prepared in various conditions, and FO water fluxes and salt passages of polyamide thin-film/CPSF composite membranes were measured and compared with each other. CPSF-based FO membranes showed significantly higher water fluxes (water flux in FO mode: 18 L/m<sup>2</sup> h, salt passage: 2.2 g/m<sup>2</sup> h under 1 M MgCl<sub>2</sub> as a draw solution, active layer facing DI water) than PSF-based FO membranes (10.5 L/m<sup>2</sup> h, 1.5 g/m<sup>2</sup> h at the same conditions), which might be due to enhanced hydrophilicity and reduced ICP.

© 2013 Crown. Published by Elsevier B.V. All rights reserved.

## 1. Introduction

Polyamide thin-film composite (PA TFC) membranes, which are mostly used as reverse osmosis (RO) membranes, consist of selective, thin polyamide layers and microporous support membranes [1]. These membranes dominate the current RO market (> 95%) because of their high flux and salt rejection compared with cellulose-based RO membranes. Forward osmosis (FO) has recently been highlighted because of its many advantages, including reduced energy requirements [2,3]. FO principally operates due to net osmotic pressure caused by differences in the water and salt activities between the feed and draw solutions. This is unlike RO, which requires high external pressure to overcome osmotic pressure. New FO membranes have been extensively developed including nanomaterial composite membranes [nanofiber, zeolite, CNT], but many studies have focused solely on the chemical and physical modification of conventional RO membranes, such as PA TFC membranes [4–6] and cellulosic membranes [7–9]. During the last decade, numerous membranes have been evaluated for FO

membrane processes, and the key factors that affect FO performance have been studied to develop new FO membranes [10–14]. However, a few membranes (e.g., cellulose based FO membranes) have been commercialized because of their high rejection properties and mechanical stability even though it has low water flux. Generally, mechanically stable, highly porous, thin support membranes with selective active layers in the form of composite or asymmetric membranes are pursued for practical applications.

PA TFC membranes have been largely studied for FO membrane processes. However, conventional PA TFC membranes for RO exhibit some drawbacks, including dense and thick membrane structures. The primary problem is low water flux, which is caused by a net osmotic pressure difference across the membrane that is significantly lower than the theoretical osmotic pressure [15]. This phenomenon occurs mainly because of internal concentration polarization (ICP) due to microporous support membrane structures or wettability [16].

Hydrophilic surface or bulk modifications have been extensively investigated to overcome the low water flux and fouling problems of hydrophobic polysulfone (PSF) membranes [17,18]. Chemical modifications, such as amination [19–21], sulfonation [22–24], carboxylation [25–27], and copolymerization with hydrophilic polymers [28–30] have been used to impart hydrophilicity

\* Corresponding author. Tel.: +82 2 2220 2338; fax: +82 2 2291 5982.  
E-mail address: [badtzhb@hanyang.ac.kr](mailto:badtzhb@hanyang.ac.kr) (H.B. Park).

to hydrophobic PSF. To decrease the ICP effect in FO membranes, not only the membrane surface but also internal pores of the porous support layer should be hydrophilic [16]. Therefore, the entire modification of hydrophobic support layer material may be required to increase the water flux of the FO membranes. Meanwhile, hydrophilic modified polymers usually show increased the degree of swelling by water and mechanical instability. Highly swollen polymers are not preferred as a support layer material since the swollen membrane structure can lead poor membrane stability. Thus, mechanically stable, hydrophilic modifications of membrane materials are required for preparing the support layer for FO membranes. For these reasons, carboxylated PSF (CPSF), which is considered to be a hydrophilic, microporous support membrane, was used to prepare PA TFC composite membranes for FO in this work. CPSF will not suffer from severe water swelling because of its low water absorption properties (12 wt%, for degree of substitution=1.9 [25]).

In this study, carboxylated polysulfones (CPSFs) were synthesized as supporting membrane materials for FO membranes. Previously, Guiver et al. [25] reported the carboxylation of polysulfone (PSF) via a direct lithiation method followed by carbon dioxide and acid treatment. The chemical [25,31,32] and separation properties of these materials as RO and UF membranes [26,27] have been reported in the literature. Here, CPSFs were prepared as new supporting membrane materials for FO membranes. Carboxylic acid groups in CPSF can improve the wettability of hydrophobic PSF [25]. The mechanical properties, water affinity, and membrane formation structure of CPSF were examined to elucidate its potential application as a new FO membrane. Here, FO membranes were prepared via interfacial polymerization of polyamide thin-film on PSF (as a control) and CPSF support layers. In addition, the correlation between support layer properties and FO performance is discussed in detail.

## 2. Experimental

### 2.1. Synthesis of carboxylated polysulfone (CPSF) and CPSF dense membranes

The synthesis procedure for CPSF is schematically illustrated in Fig. 1 [25]. A specific amount of *n*-butyllithium was added dropwise to 10 wt/vol% PSF (Udel P-3500, BP Amoco,  $M_w=80$  kg/mol) solution in THF at  $-50$  °C. After the lithiation procedure, excess  $\text{CO}_2$  dry ice was added to the reaction mixture. The precipitated lithium salt form (PSF-COOLi) of the polymer was washed with

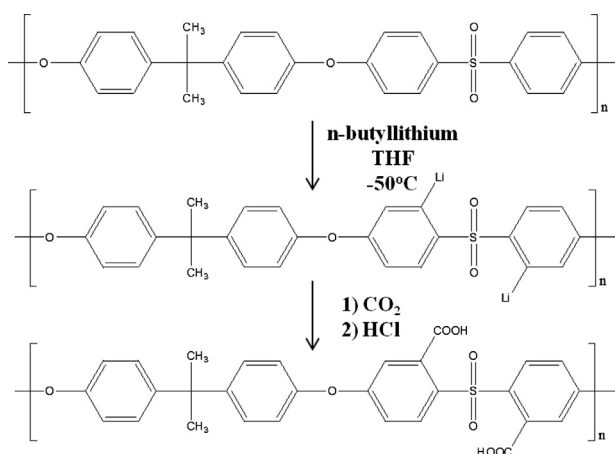


Fig. 1. Carboxylated polysulfone (CPSF) synthesis procedures [25].

ethanol. The acid form of the polymer (PSF-COOH) was then obtained by reaction with dilute hydrochloric acid. The final product was dried and stored in a vacuum oven at  $60$  °C until membrane preparation. The degree of substitution (DS) (carboxyl groups per repeat unit) was changed from 0.49 to 0.85 via molar ratios of *n*-butyllithium and polysulfone. The DS values of CPSF were confirmed by  $^1\text{H}$  NMR spectroscopy [25].

CPSF polymer powders were dissolved in dimethylacetamide (DMAc) at 20 wt% and stirred overnight to obtain a homogeneous cast solution. The prepared dope solution was thoroughly degassed in a sonication bath and stored at  $5$  °C to remove residual air bubbles before membrane casting. The dope solutions were cast on clean glass plates and placed in a  $60$  °C oven overnight. The temperature increased stepwise up to  $120$  °C, and a vacuum was then applied for 12 h to prepare the CPSF dense membranes. After natural cooling, CPSF dense membranes were rinsed to eliminate residual solvent and stored in deionized water for 24 h. The CPSF membranes were stored and dried in a  $60$  °C vacuum oven for 48 h before characterizations.

### 2.2. Preparation of PSF and CPSF microporous support layers

PSF and CPSF were dissolved in common organic solvents (i.e., dimethylformamide (DMF), DMAc) at 15 wt% and stirred overnight. Degassed dope solutions were cast on the clean glass plate using a  $150$   $\mu\text{m}$ -thick doctor knife. After membrane casting, the phase inversion process was performed in a  $25$  °C water bath. As a result, microporous PSF and CPSF membranes were successfully prepared. The microporous PSF and CPSF membranes were completely washed and stored in water before use.

### 2.3. Membrane characterizations

The mechanical properties of PSF and CPSF dense membranes were measured using a universal testing machine (AGS-J-500 N, Shimadzu, Kyoto, Japan). To compare the mechanical properties of CPSF in dry and wet states, hydrated membranes were also prepared by immersing CPSF membranes in deionized water for 48 h. The dry and wet membranes were cut into test coupons ( $2 \times 13$  mm<sup>2</sup>) using customized cutting equipment. The effective membrane thickness was measured using a hand-held thickness gauge (Absolute 547-401, Mitutoyo, Kawasaki, Japan). Tensile strength (MPa) and elongation at maximum stress (%) were measured from the average values of five samples.

Membrane samples were stored in deionized water for 48 h to measure water uptake and membrane porosity. After sufficient soaking, the weight of wet polymer membranes was measured after wiping to remove excessive water droplets on the membrane surface. Water uptake was calculated from the ratio of absorbed water and polymer in the dry state as follows:

$$\text{Water uptake (\%)} = \frac{w_{\text{wet}} - w_{\text{dry}}}{w_{\text{dry}}} \times 100 \quad (1)$$

where  $w_{\text{wet}}$  and  $w_{\text{dry}}$  are the weight of polymer in wet and dry states, respectively. The average porosities of porous membranes were calculated from the equation below [6]:

$$\text{Average porosity (\%)} = \frac{(w_{\text{wet}} - w_{\text{dry}}) / \rho_{\text{water}}}{(w_{\text{wet}} - w_{\text{dry}}) / \rho_{\text{water}} + w_{\text{dry}} / \rho_{\text{polymer}}} \times 100 \quad (2)$$

where  $\rho_{\text{water}}$  and  $\rho_{\text{polymer}}$  are the densities of water (1 g/ml) and polymer, respectively. The densities of PSF and CPSF were measured using a top-loading electronic balance (XP205, Mettler-Toledo, Switzerland) coupled with a density kit.

Attenuated total reflectance – infrared (ATR-IR) spectroscopy (Nicolet 6700 FT-IR spectrometer, Thermo scientific, Marietta, OH,

USA) and X-ray photoelectron spectroscopy (XPS) (Quantum 2000, Physical electronics, Chanhassen, MN, USA) were used to analyze the surface composition of CPSF dense and microporous membranes. The contact angle of membrane samples was measured using a contact angle instrument (Pheonix 300, SEO, Suwon, Korea). Dried membrane samples were placed on a flat plate, and the same volume of water was dropped from a syringe onto each sample. Contact angle images were taken immediately, and contact angle values were averaged from five different locations.

The cross-sectional morphologies of prepared microporous membranes were observed using field-emission scanning electron microscopy (Thermal FE-SEM, JSM-700 F, JEOL, Tokyo, Japan). To observe the cross-section morphologies, wet membrane samples were freeze-fractured in liquid nitrogen and dried. The images were taken at a resolution of  $1000 \times$ .

The hydraulic water fluxes of microporous PSF and CPSF membranes were measured by dead-end filtration. Deionized water was continuously fed to the stirred filtration cell (Amicon 8050, Millipore, Billerica, MA, USA) at a feed pressure of 1 bar using a  $N_2$  cylinder. The permeated water was automatically weighed using a digital mass balance (PAG4102C, Ohaus, Parsippany, NJ, USA) connected to a personal computer, which was used to calculate water flux.

#### 2.4. Polyamide (PA) thin-film-CPSF composite membranes

For the FO experiment, polyamide (PA) thin-film composite (TFC) membranes were prepared by interfacial polymerization on previously prepared microporous membranes. The microporous CPSF membranes were placed on an acrylic plate with a glass frame, and 3 wt% aqueous *m*-phenylenediamine (MPD) solution was then poured on the microporous membrane surface. After soaking for 3 min, the MPD solution was removed and excessive droplets were wiped from the membrane surface with a rubber roller. Trimesoylchloride (TMC) solution in dodecane (0.1 wt/vol%) was immediately poured on the membrane surface, and a polyamide thin-layer immediately formed on microporous CPSF membranes. After allowing sufficient time for interfacial polymerization, the TMC solution was removed. The resultant PA TFC membranes were rinsed several times with hexane and isopropanol, and then stored in deionized water until use.

#### 2.5. Forward osmosis (FO) measurement

Water flux and salt passage through the PA TFC membranes in FO mode were measured with lab-built cross-flow FO equipment. The membranes were placed into a membrane cell (effective membrane area =  $42 \text{ cm}^2$ ) with the active layer facing feed solution in FO mode, and facing draw solution in pressure-retarded osmosis (PRO) mode. Deionized water and 1 M  $MgCl_2$  were used as feed and draw solutions, respectively. The cross-flow rate was fixed at 1.5 L/min, and there was no external hydraulic pressure ( $\Delta P = 0$ ) for both feed and draw solutions. Weight and conductivity changes were monitored and automatically recorded by a digital mass balance (PAG4102, Ohaus, Parsippany, NJ, USA) and conductivity meter (inoLab 720, WTW, Weilheim, Germany), respectively. The water flux and salt passage in both FO and PRO modes were calculated using the following equation:

$$J_W = \frac{\Delta W_{feed} \cdot \rho_w}{A \cdot \Delta t} \quad (L/m^2 \text{ h}) \quad (3)$$

$$J_S = \frac{\Delta C_f \cdot V_f}{A \cdot \Delta t} \quad (g/m^2 \text{ h}) \quad (4)$$

where  $J_W$  is the water flux,  $\Delta W_{feed}$  is the weight change of feed solution,  $\rho_w$  is the density of water (approx. = 1 g/ml),  $A$  is the

membrane area,  $J_S$  is the salt passage,  $\Delta C_f$  is the concentration change of feed solution, and  $V_f$  is the volume of feed solution.

### 3. Results and discussion

#### 3.1. Effect of carboxylation on membrane properties

Hydrophilic modified FO membranes generally show greatly improved FO water fluxes because the hydrophilic nature of microporous support layers can alleviate the ICP effect by increasing water and salt diffusivities in the support layer [16,33]. However, the methods of hydrophilic modification of polymers (e.g., grafting, blending, and copolymerization with hydrophilic moieties) often lead to mechanical failure due to excessive swelling in a hydrated state [34]. The mechanical properties of CPSF dense membranes are compared with those of dense PSF membrane in Fig. 2(a). The tensile strength of dense membranes slightly decreases with increasing DS from 78ly decreases with

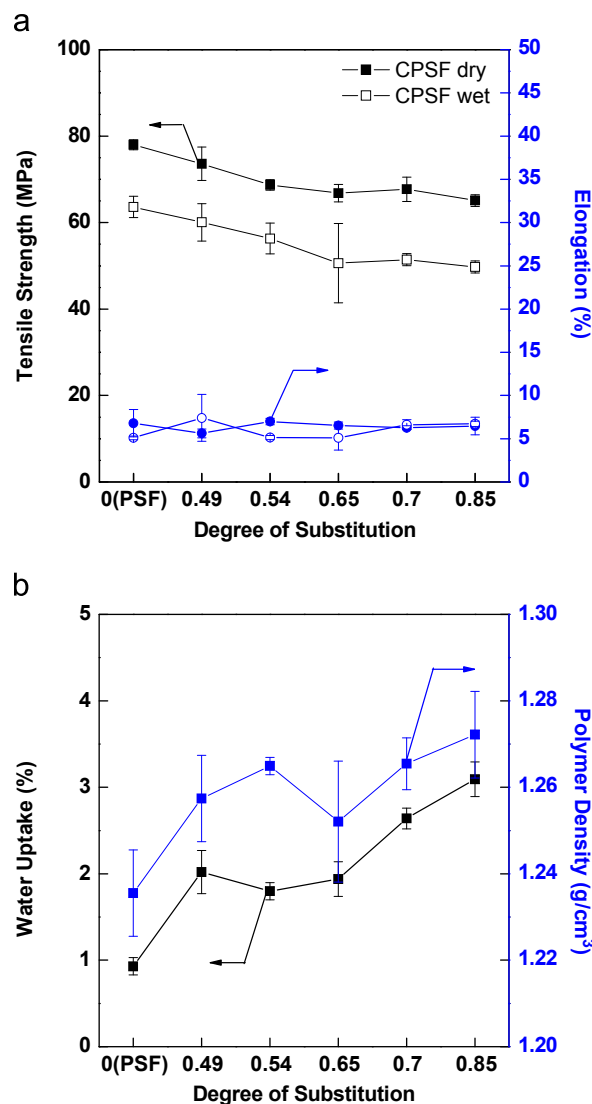


Fig. 2. Effect of degree of substitution on (a) mechanical properties of dry and wet states and (b) water uptake of CPSF dense membranes. Values were taken from average of five different tests. Weights of wet polymer membranes were measured after 48 h soaking in deionized water and dried membrane weights were obtained after 48 h drying in  $80^\circ \text{C}$  vacuum oven.

increasing DSEfCarboxylic acid groups on PSF backbones can reduce the tensile strength, since such polar groups increase the chain stiffness and packing density of the amorphous PSF. These groups also reduce the flexibility of the polymer chain by contributing to thermal motion. In addition, the mechanical strength of CPSF in the wet state is not greatly reduced, since swelling is not significant.

The water uptake of CPSF dense membranes is shown in Fig. 2(b). The introduction of carboxylic acid groups improves the water affinity of hydrophobic PSF membranes, since polar functional groups such as hydroxyl, carboxylic acid, and sulfonic acid groups can interact with water via hydrogen bonding. After PSF carboxylation, water uptake increases with increasing DS from 0.93% (DS=0) to 3% (DS=0.85). The acidity of carboxylic acid groups is lower than that of sulfonic acid groups, and carboxylic acids usually exist as dimeric pairs due to their tendency to “self-associate” via hydrogen bonding [35].

The water swelling behavior of polymers also affects the mechanical strength of microporous membranes prepared by phase inversion processes. In general, membranes used for water purification and desalination should be mechanically stable and maintain a porous structure in aqueous environments. Excessive swelling of hydrophilic membrane materials often causes pore shrinkage (i.e., swelling of pore walls), membrane breakage, and poor membrane performance. Highly swollen polymers are not suitable as support membrane materials, and other techniques are needed to retain mechanical stability even with high water affinity.

The contact angles and surface zeta potential of microporous CPSF membranes are shown in Fig. 3. The contact angle of the microporous CPSF membrane surface is lower than that of PSF membrane (65°), indicating better wettability. Conversely, the contact angles of CPSF membranes increased from 51° to 66° with increased DS from 0.49 to 0.85. That is, wettability was reduced with higher DS. Fig. 4(a) shows the intensity of carbonyl (C=O) bend (1740 cm<sup>-1</sup>) from carboxylic acid groups in the ATR spectra of membrane surfaces. The peak intensity which represents the compositions of carboxyl groups on the membrane surface linearly increases with DS from 1.8% for CP49 to 3.1% for CP85.

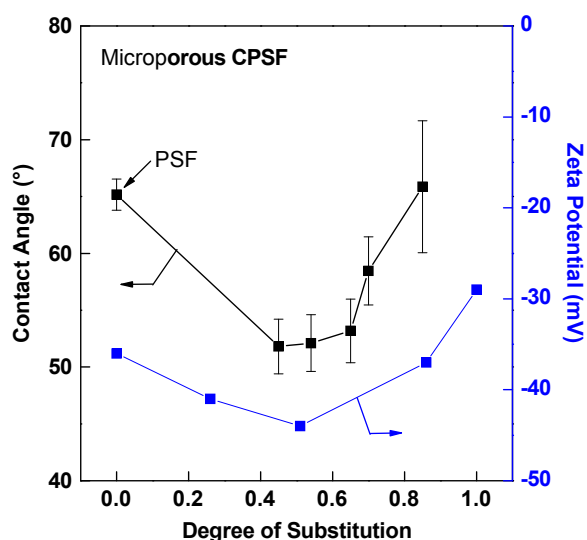


**Fig. 3.** Surface contact angle and surface zeta potential (at pH 6) of CPSF porous support layers. Values were obtained within 3 s after dropping, and average of five different locations were taken. The zeta potentials of the porous CPSF membranes at pH 6 obtained by tangential flow streaming potential measurement of porous CPSF membranes in 1 mM KCl aqueous solution are reproduced from the literature [33].

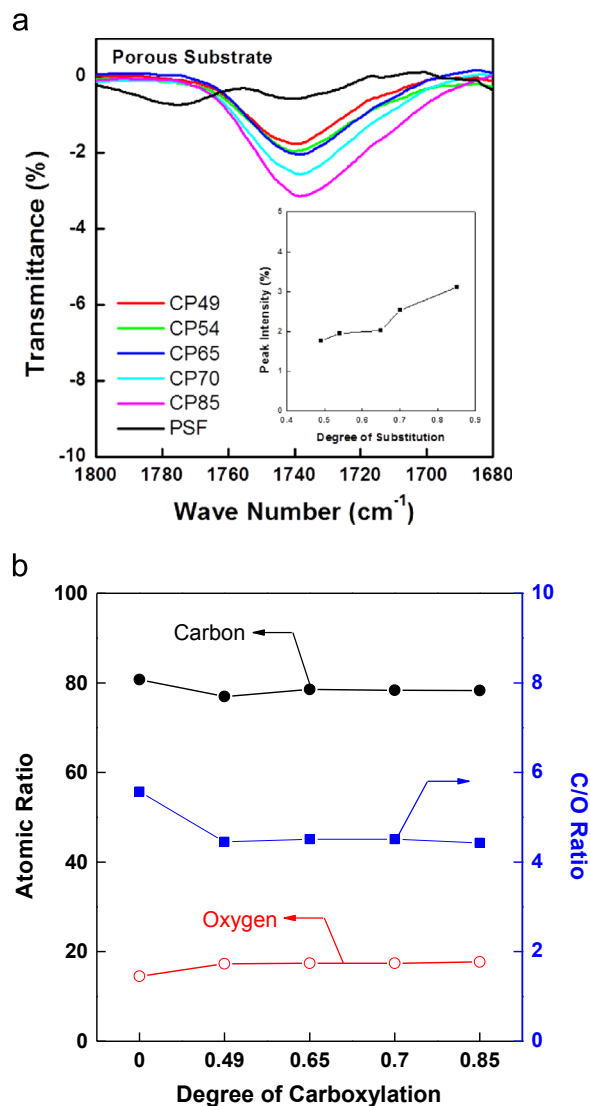


**Fig. 4.** (a) ATR-IR spectra of PSF and CPSF porous membrane surface. (b) Atomic compositions of carbon and oxygen at PSF and CPSF porous membrane surfaces from XPS analysis.

Fig. 4(b) shows the atomic ratio of carbon and oxygen on the membrane surface from XPS analysis. Due to carboxylic acid groups, the oxygen concentrations on the CPSF membrane surfaces (17.3–17.7%) are higher than that of PSF membrane surface (14.5%). In nonsolvent (water)-induced phase separation processes, the porous membrane dense surface is formed in contact with water. Hydrophilic parts are mainly located on the membrane surface due to hydrophilic interactions with water. Therefore, carboxylic acid groups tend to move on the membrane surface. Although the surface concentration of carboxylic acid groups increases with DS, the surface contact angle also increases with DS in CPSF porous membranes. Such trends in the contact angles of microporous CPSF membranes correlate with that of the surface streaming zeta potential of CPSF at pH 6. The zeta potentials of the porous CPSF membranes at pH 6 obtained by tangential flow streaming potential measurement of porous CPSF membranes in 1 mM KCl aqueous solution are reproduced from the literature [31] and presented in Fig. 3 for comparison. The dissociation of carboxylic acid groups might affect the surface charge density of CPSF. Therefore, the surface charge of CPSF in acid form is more negative at lower DS ranges. However, the surfaces of CPSF membranes with high DS will be swollen with water [31]. As a result, the

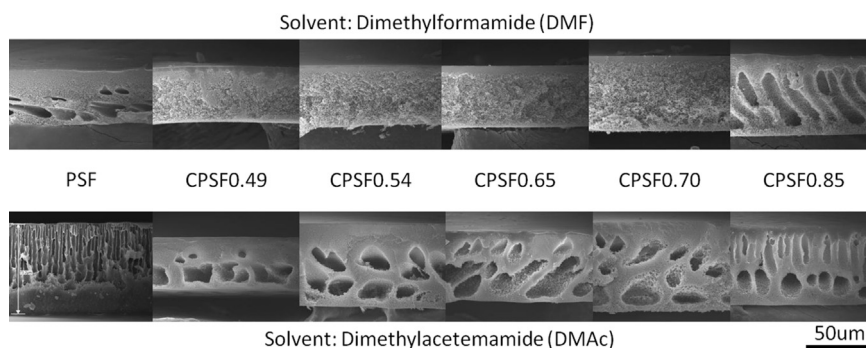


Fig. 5. Effect of solvent and DS on CPSF based support layer morphologies; polymer: 15 wt%, solvent: 85 wt%, casting thickness: 150  $\mu\text{m}$ .

electrokinetic shear plane moves far from the membrane surface, resulting in reduced membrane surface potential. The reduced surface charge density with high DS CPSFs increases the contact angle of the membrane surface.

### 3.2. Structures of CPSF membranes

A ternary phase diagram of different CPSF/solvent/water mixtures can be found in the literature [32]. The solubilities of CPSF in various organic solvents are similar to those of PSF. Water content at the cloud point increases with increasing DS in CPSF due to enhanced hydrophilicity caused by more carboxylic acid groups. As shown in Fig. 5, sponge-like structures mainly appear in microporous CPSF membranes due to slightly delayed demixing. The straight finger-like macrovoids in CPSF/DMAc membranes disappear, since the cloud point of CPSF in polymer/solvent/water systems is higher than PSF, as seen in the ternary phase diagram of CPSF [32]. However, macrovoid formation again occurs at high DS CP85 in both DMAc and DMF-induced microporous membranes. With increasing hydrophilicity, the chemical affinity between water and polymer is more favorable. As a result, large macrovoids form due to the swelling of coagulated polymer.

The structural parameters of the support layer (i.e., porosity, tortuosity, and thickness) severely affect the transport of water and salt in FO membranes. The average porosities and thicknesses of PSF and CPSF membranes are shown in Fig. 6(a). The porosity of PSF membranes are about 70%, while CP85 membranes show 84.5% of porosity. The thickness also increases with DS from 40  $\mu\text{m}$  for PSF to 68  $\mu\text{m}$  for CP85. Both porosity and thickness tend to increase with DS due to membrane swelling in phase inversion processes. The average structure parameters of PSF and CPSF membranes calculated from average porosity, theoretical tortuosity ( $\tau = 1 - \ln \epsilon^2$ ) [36], and thickness are shown in Fig. 6(b). The structural mass transfer resistances of CPSF membranes are higher than those of PSF membranes, with the exception of low DS CP49. This is because thickness generally has a greater effect on structure parameters than porosity.

The pure water fluxes of PSF and CPSF support layers under hydraulic pressure are shown in Table 1 along with the water fluxes of their PA-TFC membranes in FO and PRO modes. The water fluxes of hydrophilic CPSF support membranes are over four times higher than those of PSF support membranes. Since water permeation through porous substrates is strongly affected by membrane porosity, pore size, tortuosity, thickness, and hydrophilicity [37], the relative mass transfer resistance in support membranes is estimated by hydraulic water flux. CP49 showed the highest water flux among CPSF support membranes, but water flux decreased with DS, as the swelling of microporous CPSF membrane structures might reduce membrane pore size and increase overall membrane thickness.

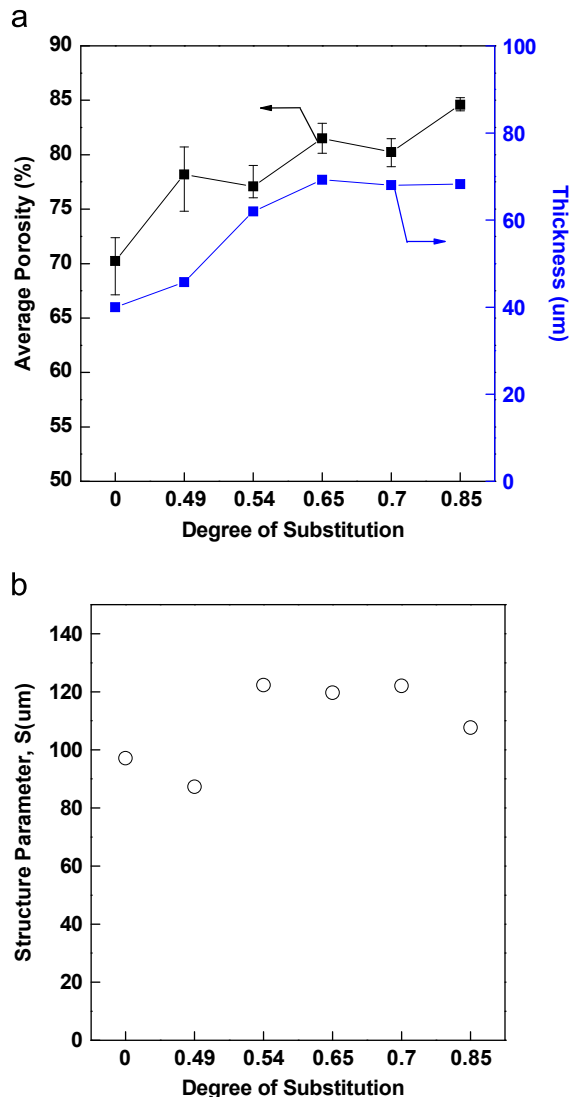


Fig. 6. (a) Average porosity and membrane thickness of PSF and CPSF membranes; polymer, 15 wt%; DMF, 85 wt%; casting thickness, 150  $\mu\text{m}$ . (b) Membrane structure parameter calculated with average porosity, thickness, and theoretical tortuosity of PSF and CPSF membranes.

### 3.3. Interfacial polymerization of polyamide on CPSF membranes

Interfacially polymerized PA active layers were formed on top of prepared PSF and CPSF support layers. In interfacial polymerization procedures, the support layers were soaked with a MPD/water solution. Adsorbed MPD molecules in the wet support layer

diffused out and reacted with TMC to form a thin PA layer at the membrane and organic solvent interface. Although reactions between carboxylic acid and diamine do not occur in ambient conditions, carboxylic acid groups on the CPSF membrane surface interacted strongly with MPD monomers, resulting in delayed interfacial polymerization reactions. In addition, the support layer surface properties can also affect on the PA layer formation [38].

**Table 1**

Comparison of water fluxes of CPSF support layers<sup>a</sup> and FO, PRO water fluxes of PA-CPSF TFC membranes.

Water flux	PSF	CP49	CPSF65	CP85
Hydraulic water flux <sup>b</sup> (L/m <sup>2</sup> h/bar)	500	3500	2500	2000
FO flux <sup>c</sup> (L/m <sup>2</sup> h)	10.5	14.3	17.9	13.1
PRO flux <sup>c</sup> (L/m <sup>2</sup> h)	23.2	25.1	27.5	28.6

<sup>a</sup> Polymer concentration: 15 wt% in DMF, membranes were cast on glass plates and directly immersed in water coagulation bath.

<sup>b</sup> Test condition: dead-end filtration at 25 °C and 1 bar; deionized water was used as feed solution.

<sup>c</sup> Test condition: cross-flow FO measurement, feed solution: D.I. water, draw solution: 1 M MgCl<sub>2</sub>.

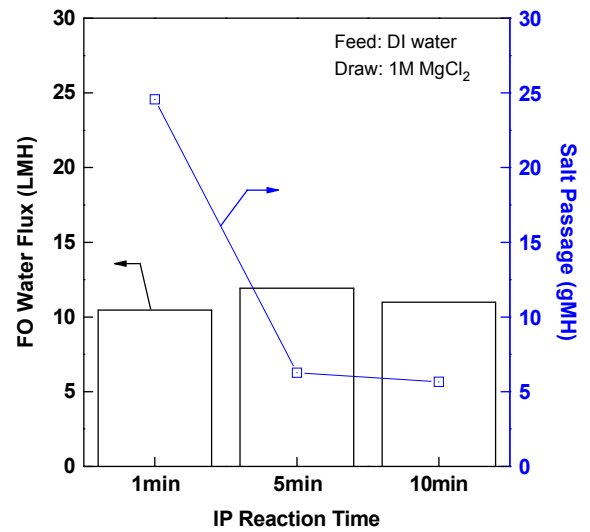


**Fig. 8.** Effect of interfacial polymerization reaction time on FO performances, support layer: CP49, 15 wt%; solvent, DMAc, 85 wt%; casting thickness, 150  $\mu$ m; active layer, 3 wt% MPD/water, 0.1 wt/vol% TMC/dodecane, FO experiment: feed solution: D.I. water, draw solution: 1 M MgCl<sub>2</sub>.

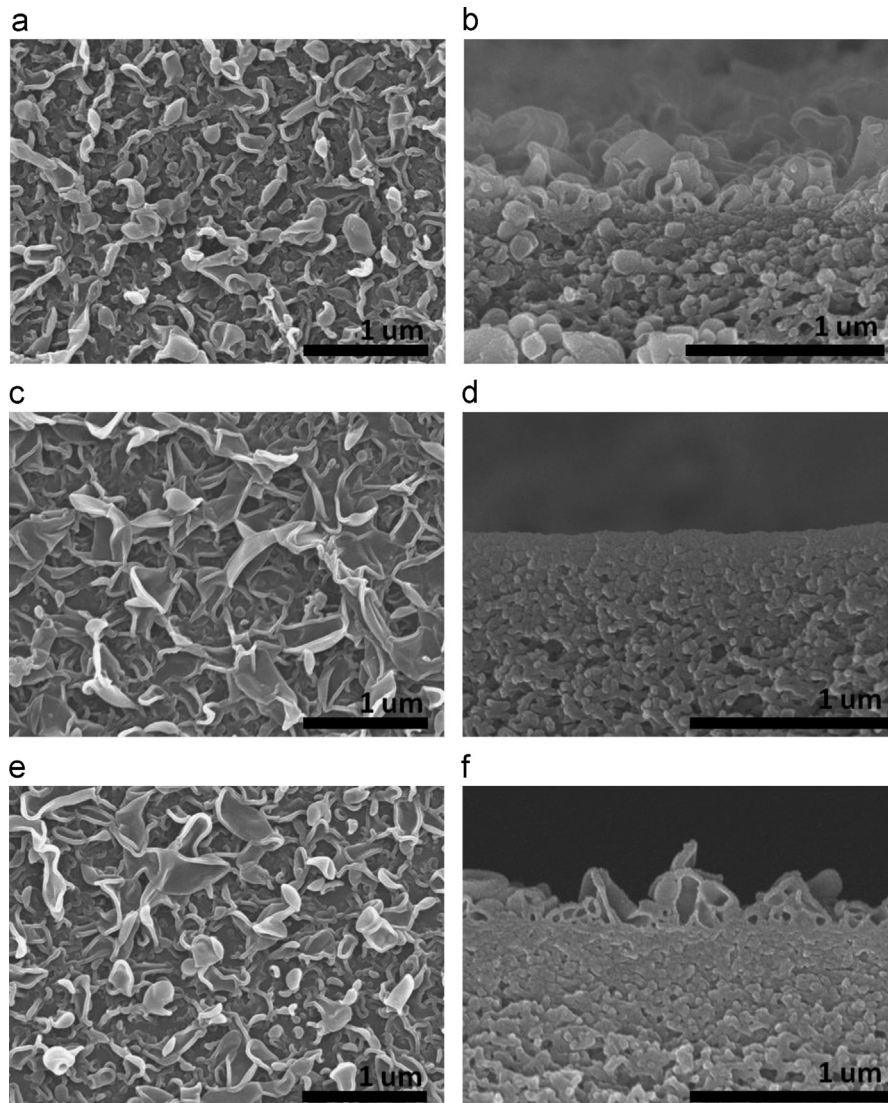


**Fig. 7.** Surface and cross-sectional morphologies of PA-PSF (a, b), PA-CP49 (c, d), PA-CP49 (10 min reaction), and (e, f) TFC membranes.

For the hydrophobic support layer surfaces with small surface pores, the relatively thin, rough PA layer tend to be formed on the membrane surface since the interface between organic phase and aqueous phase are generally placed on the surface pores. For the hydrophilic support layer surfaces with large surface pores, however, the interface could be placed in the surface pores resulting thick, loose PA layer with relatively smooth surface roughness. Therefore, the control of PA layer formation is needed to prevent the leakage of draw solute and to sustain high water/salt selectivity for hydrophilic modified support layers.

Surface and cross-sectional SEM images of PA layers on PSF and CPSF membranes are shown in Fig. 7. PA layers (100–200 nm thick) were successfully formed on PSF porous substrates. PA layers on CPSF porous membranes have a relatively loose ridge and valley structure in the general interfacial polymerization reaction time (1 min). As reaction time increases, more stable and dense PA layers (200–300 nm) were formed on CPSF membranes.

The effect of interfacial polymerization reaction time on the FO performance of PA-CPSF TFC membranes is illustrated in Fig. 8. Salt passage strongly depends on the water/salt selectivity of the active

layer. Salt passage dramatically decreased with increased reaction time for PA-CPSF TFC membranes. By increasing the interfacial polymerization reaction time, denser PA layers were formed due to increased amounts of amine monomers diffusing to the organic phase [39]. FO water flux did not change despite improved selectivity of the PA layer. Mass transfer resistance due to ICP in the support layer, rather than resistance of the active layer, is the main obstacle for water permeation. Because of this, the severe salt passage in high flux FO membranes can be effectively reduced by enhancing the selectivity of the active layer without sacrificing water flux.

### 3.4. FO performances of PA-CPSF TFC membranes

The FO performances of PA-CPSF TFC membranes are compared with those of PA-PSF TFC membranes in Fig. 9. Water fluxes in the FO and PRO modes increased with DS. Similar to the trend for the water flux of porous substrates, FO water flux decreased with highly substituted CP85. FO water flux is generally much lower than the theoretical value (calculated from water permeability in RO mode) due to the ICP effect. If the support layer has a low mass transfer resistance for water and draw solute, water flux will increase due to the reduction in the ICP effect. PA-TFC membranes based on microporous CPSF membranes prepared from DMAc and DMF exhibited higher FO and PRO water flux than PSF-based TFC membranes due to decreased structural mass transfer resistance and improved hydrophilicity. The water flux differences between FO and PRO modes were less significant in PA-CPSF membranes due to lower water and solute transport resistance in microporous CPSF support membranes. However, FO water flux is lower for CP85 membranes than for CP65 membranes due to the membranes swelling with water.

Draw solute passage generally increases along with water flux in FO and PRO modes, since a reduction in the ICP effect increases the effective concentration difference at the active layer. A strong trade-off relationship between FO water flux and draw solute retention ( $1/J_s$ ) has been reported in the literature, as shown in Fig. 10. The water flux and salt passages in the literature were taken at the same

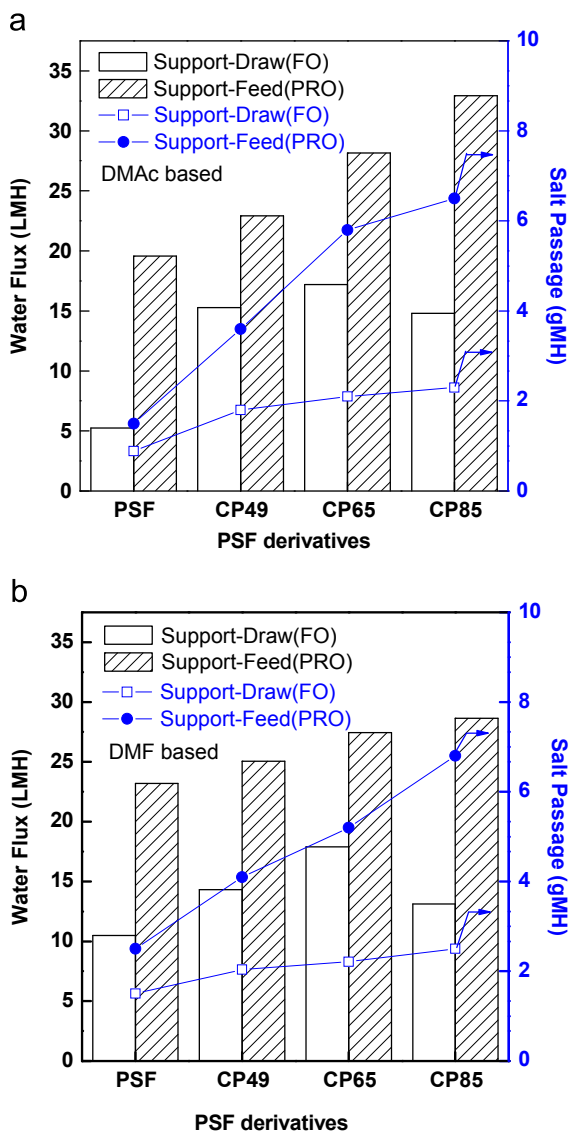


**Fig. 9.** FO performances of (a) DMAc based and (b) DMF based CPSF membranes; support layer, polymer: 15 wt%; solvent, 85 wt%; casting thickness, 150  $\mu\text{m}$ ; active layer, 1.5 wt% MPD/water and 0.05 wt/vol% TMC/dodecane; IP reaction time, 10 min; FO experiment: feed solution, D.I. water; draw solution, 1 M  $\text{MgCl}_2$ .

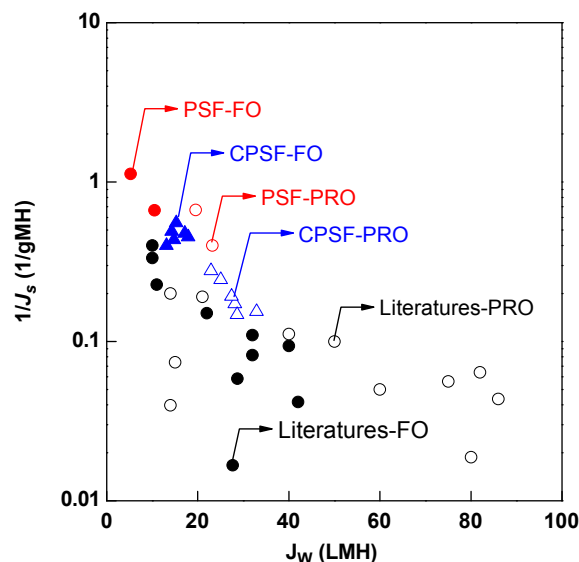


**Fig. 10.** Tradeoff relationship between water flux and draw salt rejection. Comparison of FO performances of PA-PSF (red) and PA-CPSF (blue) prepared in this study with recently reported FO membrane performances (black) at the same experimental conditions (Feed, DI water; Draw, 1 M  $\text{MgCl}_2$ ) from the literature [8,9,40–43]. (For interpretation of the references to color in this figure caption, the reader is referred to the web version of this article.)

experimental conditions (i.e., DI water as a feed solution, 1 M MgCl<sub>2</sub> as a draw solution). When water flux was increased by reducing the ICP effect, salt passage also generally increased. This effect was due to an increase in the concentration gradient between the inner and outer surface of the active layer (i.e., the driving force of salt diffusion). A more selective active layer is needed to reduce draw solute passage in high water flux FO membranes. In this study, PA-CPSF FO membranes exhibited both higher water flux and draw solute rejection properties than PA-PSF FO membranes and recently reported FO membranes [8,9,40–43].

#### 4. Conclusions

Various PA TFC membranes for FO applications were prepared using PSF and CPSF as support layer materials. PSF-based polymers have properties desirable for a membrane material, such as high mechanical, chemical, and thermal stability. Although the tensile strength of CPSF slightly decreased with increasing DS, it was still high enough to warrant preparing porous membranes with CPSF for FO applications. Due to their polarity, carboxylic acid groups in hydrophobic polysulfone increase the hydrophilicity of the polymer. The hydrophilicity of CPSF affects the polymer–solvent–nonsolvent interactions that determine membrane structures. The membrane formation and structures of PSF and CPSF varied with organic solvent and DS. CPSF membranes are more favorable for a support layer for FO membranes than PSF membranes due to their high porosity and hydrophilicity. The FO water fluxes of CPSF-based membranes are higher than those of PSF-based membranes due to hydrophilicity.

#### Acknowledgments

The World Class University (WCU) Program of the Ministry of Education, Science, and Technology (MEST) in Korea supported this study.

#### References

- [1] K.P. Lee, T.C. Arnot, D. Mattia, A review of reverse osmosis membrane materials for desalination—development to date and future potential, *J. Membr. Sci.* 370 (2011) 1–22.
- [2] M. Elimelech, W.A. Phillip, The future of seawater desalination: energy, technology, and the environment, *Science* 333 (2011) 712–717.
- [3] T.Y. Cath, A.E. Childress, M. Elimelech, Forward osmosis: principles, applications, and recent developments, *J. Membr. Sci.* 281 (2006) 70–87.
- [4] N.Y. Yip, A. Tiraferri, W.A. Phillip, J.D. Schiffman, M. Elimelech, High performance thin-film composite forward osmosis membrane, *Environ. Sci. Technol.* 44 (2010) 3812–3818.
- [5] X.X. Song, Z.Y. Liu, D.R.D.L. Sun, Nano gives the answer: breaking the bottleneck of internal concentration polarization with a nanofiber composite forward osmosis membrane for a high water production rate, *Adv. Mater.* 23 (2011) 3256–3260.
- [6] J. Wei, C.Q. Qiu, C.Y.Y. Tang, R. Wang, A.G. Fane, Synthesis and characterization of flat-sheet thin film composite forward osmosis membranes, *J. Membr. Sci.* 372 (2011) 292–302.
- [7] J.C. Su, Q. Yang, J.F. Teo, T.S. Chung, Cellulose acetate nanofiltration hollow fiber membranes for forward osmosis processes, *J. Membr. Sci.* 355 (2010) 36–44.
- [8] K.Y. Wang, R.C. Ong, T.S. Chung, Double-skinned forward osmosis membranes for reducing internal concentration polarization within the porous sublayer, *Ind. Eng. Chem. Res.* 49 (2010) 4824–4831.
- [9] S. Zhang, K.Y. Wang, T.S. Chung, H.M. Chen, Y.C. Jean, G. Amy, Well-constructed cellulose acetate membranes for forward osmosis: Minimized internal concentration polarization with an ultra-thin selective layer, *J. Membr. Sci.* 360 (2010) 522–535.
- [10] W.Y. Li, Y.B. Gao, C.Y.Y. Tang, Network modeling for studying the effect of support structure on internal concentration polarization during forward osmosis: model development and theoretical analysis with FEM, *J. Membr. Sci.* 379 (2011) 307–321.
- [11] L. Shi, S.R. Chou, R. Wang, W.X. Fang, C.Y. Tang, A.G. Fane, Effect of substrate structure on the performance of thin-film composite forward osmosis hollow fiber membranes, *J. Membr. Sci.* 382 (2011) 116–123.
- [12] W.L. Tang, H.Y. Ng, Concentration of brine by forward osmosis: performance and influence of membrane structure, *Desalination* 224 (2008) 143–153.
- [13] M. Park, J.J. Lee, S. Lee, J.H. Kim, Determination of a constant membrane structure parameter in forward osmosis processes, *J. Membr. Sci.* 375 (2011) 241–248.
- [14] A. Tiraferri, N.Y. Yip, W.A. Phillip, J.D. Schiffman, M. Elimelech, Relating performance of thin-film composite forward osmosis membranes to support layer formation and structure, *J. Membr. Sci.* 367 (2011) 340–352.
- [15] J.R. McCutcheon, M. Elimelech, Influence of concentrative and dilutive internal concentration polarization on flux behavior in forward osmosis, *J. Membr. Sci.* 284 (2006) 237–247.
- [16] J.R. McCutcheon, M. Elimelech, Influence of membrane support layer hydrophobicity on water flux in osmotically driven membrane processes, *J. Membr. Sci.* 318 (2008) 458–466.
- [17] K.C. Khulbe, C. Feng, T. Matsuura, The art of surface modification of synthetic polymeric membranes, *J. Appl. Polym. Sci.* 115 (2010) 855–895.
- [18] C.S. Zhao, J.M. Xue, F. Ran, S.D. Sun, Modification of polyethersulfone membranes – a review of methods, *Prog. Mater. Sci.* 58 (2013) 76–150.
- [19] M. Rucka, G. Pozniak, B. Turkiewicz, W. Trochimczuk, Ultrafiltration membranes from polysulfone/aminated polysulfone blends with proteolytic activity, *Enzyme Microb. Technol.* 18 (1996) 477–481.
- [20] D.L. Arockiasamy, A. Nagendran, K.H. Shobana, D. Mohan, Preparation and characterization of cellulose acetate/aminated polysulfone blend ultrafiltration membranes and their application studies, *Sep. Sci. Technol.* 44 (2009) 398–421.
- [21] M.H. Chen, T.C. Chiao, T.W. Tseng, Preparation of sulfonated polysulfone/polysulfone and aminated polysulfone/polysulfone blend membranes, *J. Appl. Polym. Sci.* 61 (1996) 1205–1209.
- [22] N. Vinnikova, G.B. Tanny, Transport of Ions and Water in Sulfonated Polysulfone Membranes, ACS Symposium Series, vol. 153, 1981, pp. 351–365.
- [23] I. Jitsuhara, S. Kimura, Structure and properties of charged ultrafiltration membranes made of sulfonated polysulfone, *J. Chem. Eng. Jpn* 16 (1983) 389–393.
- [24] R. Malaisamy, R. Mahendran, D. Mohan, M. Rajendran, V. Mohan, Cellulose acetate and sulfonated polysulfone blend ultrafiltration membranes. I. Preparation and characterization, *J. Appl. Polym. Sci.* 86 (2002) 1749–1761.
- [25] M.D. Guiver, S. Croteau, J.D. Hazlett, O. Kutowy, Synthesis and characterization of carboxylated polysulfones, *Br. Polym. J.* 23 (1990) 29–39.
- [26] M.D. Guiver, A.Y. Tremblay, C.M. Tam, Reverse-osmosis membranes from novel hydrophilic polysulfones, in: Proceedings of the Symposium on Advances in Reverse Osmosis and Ultrafiltration, 1989, pp. 53–70.
- [27] D. Mockel, E. Staude, M.D. Guiver, Static protein adsorption, ultrafiltration behavior and cleanability of hydrophilized polysulfone membranes, *J. Membr. Sci.* 158 (1999) 63–75.
- [28] J.Y. Park, M.H. Acar, A. Akthakul, W. Kuhlman, A.M. Mayes, Polysulfone-graft-poly(ethylene glycol) graft copolymers for surface modification of polysulfone membranes, *Biomaterials* 27 (2006) 856–865.
- [29] Y.Q. Song, J. Sheng, M. Wei, X.B. Yuan, Surface modification of polysulfone membranes by low-temperature plasma-graft poly(ethylene glycol) onto polysulfone membranes, *J. Appl. Polym. Sci.* 78 (2000) 979–985.
- [30] Y.H. Cho, H.W. Kim, S.Y. Nam, H.B. Park, Fouling-tolerant polysulfone–poly(ethylene oxide) random copolymer ultrafiltration membranes, *J. Membr. Sci.* 379 (2011) 296–306.
- [31] D. Mockel, E. Staude, M. Dal-Cin, K. Darcovich, M. Guiver, Tangential flow streaming potential measurements: hydrodynamic cell characterization and zeta potentials of carboxylated polysulfone membranes, *J. Membr. Sci.* 145 (1998) 211–222.
- [32] W.W.Y. Lau, M.D. Guiver, T. Matsuura, Phase-separation in carboxylated polysulfone solvent water-systems, *J. Appl. Polym. Sci.* 42 (1991) 3215–3221.
- [33] J.T. Arena, B. McCloskey, B.D. Freeman, J.R. McCutcheon, Surface modification of thin film composite membrane support layers with polydopamine: Enabling use of reverse osmosis membranes in pressure retarded osmosis, *J. Membr. Sci.* 375 (2011) 55–62.
- [34] R. Guan, H. Zou, D.P. Lu, C.L. Gong, Y.F. Liu, Polyethersulfone sulfonated by chlorosulfonic acid and its membrane characteristics, *Eur. Polym. J.* 41 (2005) 1554–1560.
- [35] V. Doan, R. Koppe, P.H. Kasai, Dimerization of carboxylic acids and salts: an IR study in perfluoropolyether media, *J. Am. Chem. Soc.* 119 (1997) 9810–9815.
- [36] B.P. Boudreau, The diffusive tortuosity of fine-grained un lithified sediments, *Geochim. Cosmochim. Acta* 60 (1996) 3139–3142.
- [37] J. Mulder, Basic Principles of Membrane Technology, 2nd ed., Springer, 1996.
- [38] A.K. Ghosh, E.M.V. Hoek, Impacts of support membrane structure and chemistry on polyamide–polysulfone interfacial composite membranes, *J. Membr. Sci.* 336 (2009) 140–148.
- [39] J. Lee, A. Hill, S. Kentish, Formation of a thick aromatic polyamide membrane by interfacial polymerisation, *Sep. Purif. Technol.* 104 (2013) 276–283.
- [40] Q. Yang, K.Y. Wang, T.S. Chung, Dual-layer hollow fibers with enhanced flux as novel forward osmosis membranes for water production, *Environ. Sci. Technol.* 43 (2009) 2800–2805.
- [41] Q. Saren, C.Q. Qiu, C.Y.Y. Tang, Synthesis and characterization of novel forward osmosis membranes based on layer-by-layer assembly, *Environ. Sci. Technol.* 45 (2011) 5201–5208.
- [42] L. Setiawan, R. Wang, K. Li, A.G. Fane, Fabrication of novel poly(amide-imide) forward osmosis hollow fiber membranes with a positively charged nanofiltration-like selective layer, *J. Membr. Sci.* 369 (2011) 196–205.
- [43] C. Qui, S. Qi, C.Y. Tang, Synthesis of high flux forward osmosis membranes by chemically crosslinked layer-by-layer polyelectrolytes, *J. Membr. Sci.* 381 (2011) 74–80.